The International Journal of Advanced Manufacturing Technology (2018) 96:4407–4421
https://doi.org/10.1007/s00170-018-1611-z

ORIGINAL ARTICLE

Investigations on the surface effect of ultrasonic vibration-assisted 6063 aluminum alloy ring upsetting

Zhendong Xie[1] · Yanjin Guan[1] · Lihua Zhu[1] · Jiqiang Zhai[1] · Jun Lin[1] · Xiaohui Yu[1]

Received: 26 July 2017 / Accepted: 10 January 2018 / Published online: 25 March 2018

Abstract
The ultrasonic vibration-assisted 6063 aluminum alloy ring upsetting with different lubricants was performed to explore the effects of ultrasonic vibration on specimens during upsetting. The influence of ultrasonic vibration on upsetting was analyzed on the basis of the stress-strain curves which were obtained from different experimental conditions. The friction coefficients on the specimen/tool interface under different experimental conditions were computed according to the size of compressed specimens. The effect of ultrasonic vibration on surface quality was also investigated by analyzing the variation of surface hardness, roughness, and topography. Compared with the conventional upsetting, the true stress decreased by 14.26 and 15.45% when the amplitude was 3.34 and 3.96 μm respectively. The friction coefficient on the specimen/tool interface reduced under the effect of ultrasonic vibration, and the friction coefficient decreased with the increase of the vibration amplitude. The ultrasonic vibration improved the surface quality effectively. The surface quality, roughness, hardness, and anti-friction effect on the top surface that contacts directly with the vibration tool head were better than those on the bottom surface.

Keywords Ultrasonic vibration · Ring upsetting · Friction coefficient · Lubrication · Surface quality

1 Introduction

Nowadays, ultrasonic vibration has been widely used in metal plastic forming, including ultrasonic drawing, ultrasonic extrusion, and ultrasonic upsetting. Interesting effects occur when ultrasonic vibration is applied in the metal forming processes, including a reduction in the friction between the die and the specimen, and a decrease in the forming forces, which attracts many scholars. Yang et al. [1] applied ultrasonic vibration to the die in the process of wire drawing; the results showed that the surface quality was improved and the limited drawing ratio can be increased. Kim and Lee [2] found that the turning or cutting quality was improved under the effect of ultrasonic vibration. Ahmadi et al. [3] imposed ultrasonic vibration in the ECAP process and found superimposing ultrasonic vibration with the amplitude of 2.5 μm increases the efficiency of the ECAP process by 25.8%. Bunget and Ngaile [4] investigated the ultrasonic vibration-assisted micro-forming and obtained small parts with high surface quality. Jimma et al. [5] and Ashida and Aoyama [6] investigated the influence of ultrasonic vibration on the deep drawing process and found the limited deep drawing ratio can be increased and avoided the crack.

It can be found that previous studies mainly focus on the application of the ultrasonic vibration in various processing technology. Schey [7] classified the beneficial effects of ultrasonic vibration in manufacturing processes into two categories: reductions in strength of the material and interfacial friction. In terms of the impacts of the ultrasonic vibration on metal forming processes, they were summarized as volume effect [8–11] and surface effect [6, 12–13] respectively although internal forming mechanisms were still unclear. Friction between the workpiece and the tool plays an important role in metal forming processes. The surface effect of ultrasonic vibration has a significant impact on the lubrication condition, which leads to the reduction of the friction on the workpiece/tool interface, and improves the surface quality of the workpiece. Therefore, many scholars have done a lot of investigations on the surface effect of the ultrasonic vibration.

✉ Yanjin Guan
guan_yanjin@sdu.edu.cn

[1] Key Laboratory for Liquid-Solid Structural Evolution and Processing of Materials (Ministry of Education), Shandong University, Jinan 250061, People's Republic of China

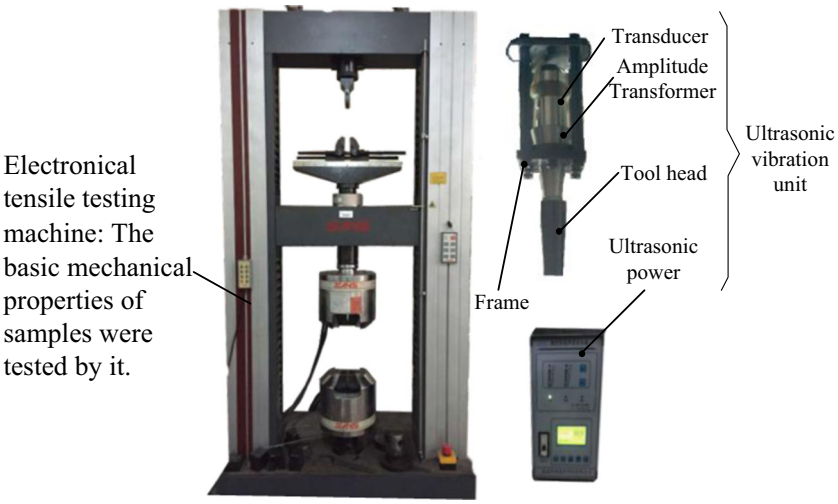

Fig. 1 Ultrasonic-assisted upsetting test system

The surface effect was separated by Siegert and Ulmer [14]; the reduction of the sliding friction between the longitudinal oscillating die and the workpiece can be explained by the so-called sliding friction vector effect. Lehfeldt and Pohlman [15] examined the feasibility of exciting a ball by the vibration on a revolving plate in experiments on the influence of the ultrasonic vibration on friction. The frictional forces were minimal at the contact surface when the direction of vibration was parallel to the direction of motion. Jimma et al. [5] applied ultrasonic vibration to the deep drawing process and showed that ultrasonic vibration deep drawing was very effective in increasing the limiting drawing ratio and surpassed the theoretical value LDR of deep drawing by ideal tools without friction. Dawson et al. [16] found that the forming quality of surface was improved under the effect of ultrasonic vibration. They considered that the friction vector was changed and the lubrication condition was improved. In the upsetting processes, the ultrasonic vibration shows the volume and surface effects at the same time. Some researchers completed basic experimental studies of ultrasonic upsetting. Huang et al.[17] used the plasticine as a model material to simulate the hot metal and found applying an ultrasonic vibration to the die reduces the mean forming force during upsetting. He concluded that the stress superposition effect and the reduction of interface friction contributed to the phenomenon above. Daud et al. [18] applied ultrasonic vibration to the bottom platen in compression tests on aluminum alloy specimens; the stress-strain relationship could be characterized by a temporary effective softening of the material during intervals of ultrasonic excitation. Abdul and Lucas [19] found that the forming force reduced under the effect of ultrasonic vibration during upsetting process. Zhuang et al. [20] found the force reduction because of stress superposition and friction effects was still less than the actual force reduction from the tests.

The surface effect of ultrasonic vibration was only qualitatively studied in the above investigations, and under different friction conditions, the change of stress-strain relationship in the process of ultrasonic vibration-assisted upsetting was studied by Daud et al. [13] Nevertheless, the other previous studies are restricted to a single lubrication condition, so that further experimental studies on the influence of the ultrasonic vibration on the friction coefficient under different lubrication conditions and the quantitative research of the surface quality, including surface roughness and topography, are insufficient. Moreover, among the methods for measuring the friction

Table 1 Chemical composition of 6063 aluminum alloy (wt%)

Element	Si	Fe	Cu	Mn	Mg	Zn	Ti	Cr	Other	Al
Content	0.32	0.35	0.1	0.1	0.6	0.1	0.1	0.1	0.05	Balance

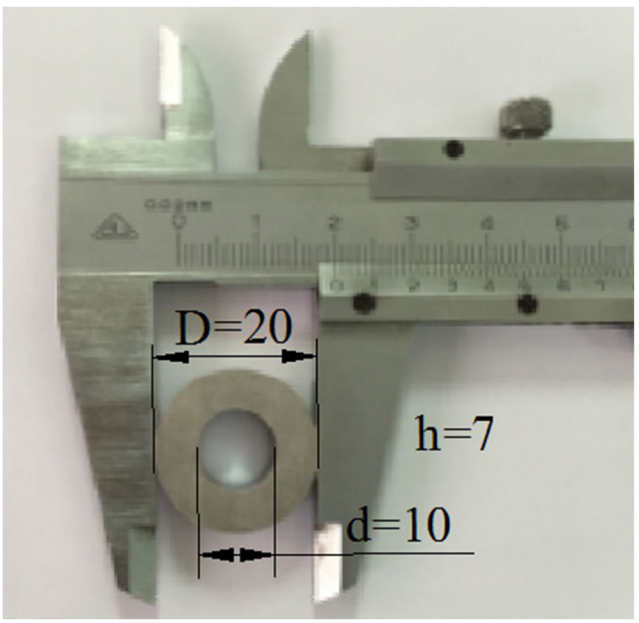

Fig. 2 Upsetting specimen

Table 2 Test schemes

Number	Amplitude (μm)	Lubricant	Duration of applying ultrasonic vibration	Reduction in height
D1	0	Dry friction	Applying vibration when the load reaches to 5 kN until the reduction in height is 3 mm	3 mm
D2	3.34	Dry friction		
D3	3.96	Dry friction		
PA4	0	Paraffin		
PA5	3.34	Paraffin		
PA6	3.96	Paraffin		
L7	0	Lithium grease		
L8	3.34	Lithium grease		
L9	3.96	Lithium grease		
PT10	0	PTFE film		
PT11	3.34	PTFE film		
PT12	3.96	PTFE film		

coefficient or the friction factor, the ring compression test has been widely employed over the last two decades [21–23]. Thus, in our work, 6063 aluminum alloy ring specimens were taken as the research object in room temperature upsetting tests. The impact of ultrasonic vibration on ring upsetting in different lubrication conditions was investigated. The effect of ultrasonic vibration on the variation of the friction coefficient under the conditions of dry friction, liquid lubrication, grease lubrication, and PTFE film lubrication, as well as the influence of ultrasonic vibration on surface topography, surface hardness, and surface roughness, was analyzed quantificationally to reveal the surface effect of the ultrasonic vibration in the ultrasonic vibration-assisted upsetting.

2 Establishment of ultrasonic vibration-assisted upsetting system and test scheme

2.1 Establishment of ultrasonic vibration-assisted upsetting system

An experimental system consists of a universal material testing machine (SANSCMT5205) and a set of ultrasonic vibration unit, as shown in Fig. 1. In the present work, the ultrasonic vibration unit includes an ultrasonic generator, transducer, amplitude transformer, and tool head. The frequency of the ultrasonic power is 15 kHz and two kinds of powers (1 and 1.4 kW) can be output. The transducer converts the high-frequency electric oscillation generated by the ultrasonic power into the mechanical vibration. However, the amplitude of the output mechanical vibration is very small, so it needs to be amplified by using the compound ultrasonic longitudinal vibrating amplitude transformer. The tool head can further make the output amplitude be amplified. Finally, the corresponding output amplitudes are 3.34 and 3.96 μm, respectively. The amplitudes were set value according to the relationship between the amplitude and the output power. The ultrasonic vibration is acted on the upsetting specimens through the tool head. In addition, the ultrasonic vibration unit is installed on the experimental machine by means of a frame.

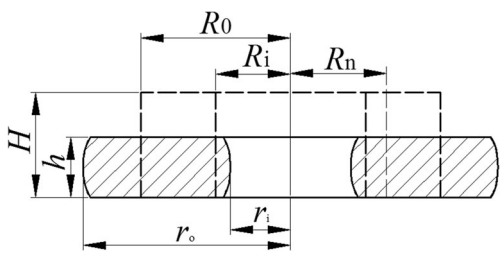

Fig. 3 Ring upsetting deformation

2.2 Compression specimens and treatment

Table 1 gives the chemical composition of the 6063 wrought aluminum alloy used in the tests.

The dimensional ratio of the standard ring upsetting specimen is 6:3:2, i.e., the external diameter, the internal diameter, and the height are 20, 10, and 7 mm, respectively, as shown in Fig. 2.

In order to eliminate the residual stress caused by machining operations and ensure the consistency of the microstructures and performances of specimens, a recrystallization annealing process was conducted for the 6063 aluminum alloy specimens. The specimens were heated to 500 °C at the heating rate of 5 °C/min and then cooled down to the room temperature in a furnace after 4 h thermal insulation. The specimens were buried in alumina powders to prevent them from oxidization during the annealing process.

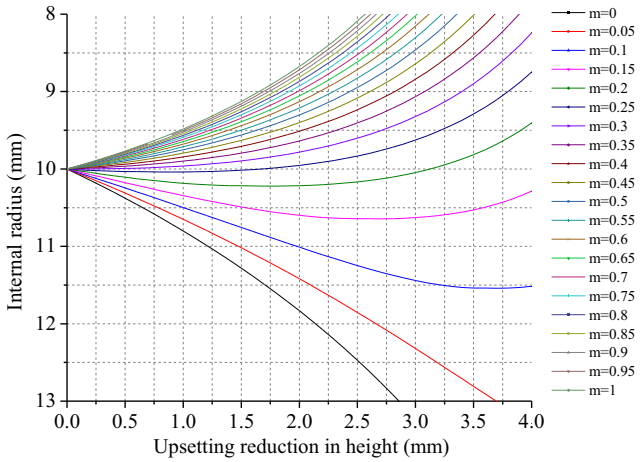

Fig. 4 Theoretical calibrating curves

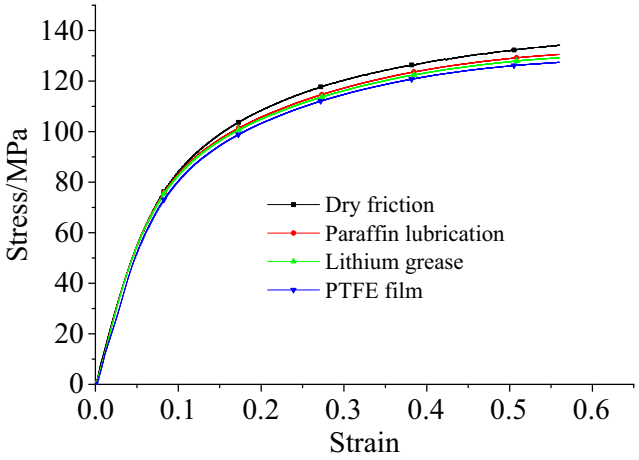

Fig. 6 The stress-strain curves of static upsetting under different lubrication conditions

2.3 Upsetting test schemes

Upsetting tests were conducted for annealed upsetting specimens of 6063 aluminum alloy under different vibrating conditions to mensurate the variation of the friction coefficient between the tool and specimen. Meanwhile, influences of the ultrasonic vibration on the deformed shape, friction coefficient, surface roughness, and surface hardness of upsetting specimens under different lubrication conditions were investigated.

In experiments, the upsetting velocity always kept 1 mm/min. All of tests were performed at the room temperature. The ultrasonic vibration was applied when the load reached to 5 kN until the reduction in height was 3 mm. Each experiment was repeated five times in order to guarantee the reliability of the experimental results. The test schemes are shown in Table 2.

2.4 Measurement method of friction coefficient

During the ring upsetting process, the deformation of ring specimens has relationship with the friction condition of the specimen/tool interface. There is a critical value of the friction coefficient; when the friction coefficient is less than the critical value, the internal and external radii of the compressed specimen increase simultaneously. When the friction coefficient is greater than the critical value, there is a neutral layer within the ring. During deformation, the material within the neutral layer flows inwards and makes the internal radius decreased while the material outside the neutral layer flows outwards and causes the increase of the external radius, as shown in

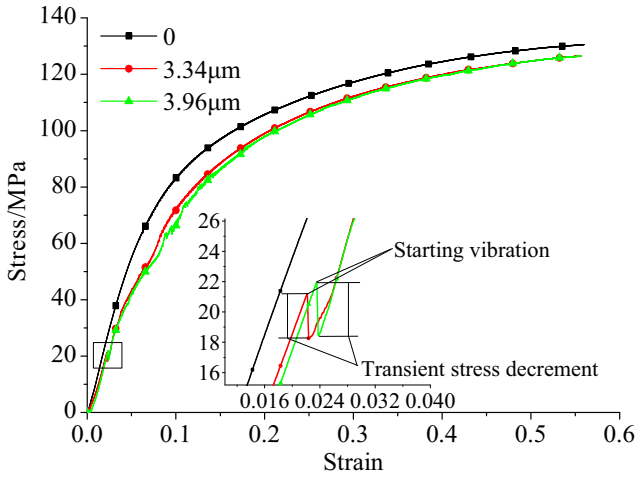

Fig. 5 The stress-strain curves of upsetting under dry friction condition

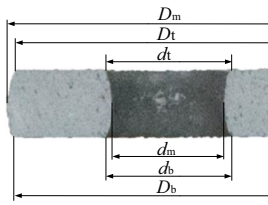

(a) The characteristic dimensions of the final profiles

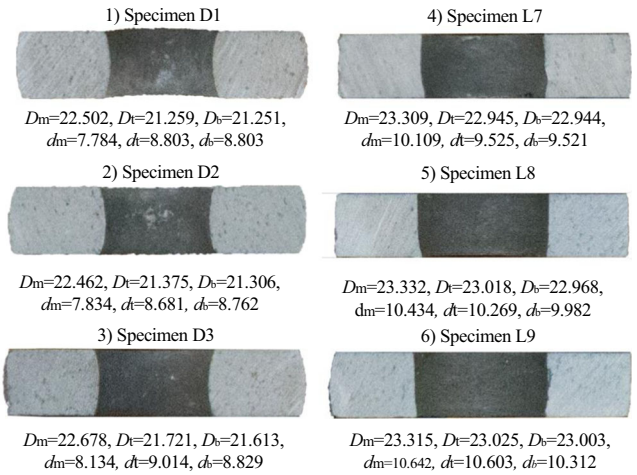

(b) The cross-sectional profiles

Fig. 7 The cross-sectional profiles of the specimens for static upsetting and vibration upsetting under dry friction condition and paraffin-lubricated condition. **a** The characteristic dimensions of the final profiles. **b** The cross-sectional profiles

Table 3 The λ of compressed specimens under dry friction condition

Amplitude (μm)	λt	λb	$\lambda' t$	$\lambda' b$
0	$0.893 \pm 1.92 \times 10^{-3}$	$0.891 \pm 2.86 \times 10^{-3}$	$1.279 \pm 1.92 \times 10^{-3}$	$1.279 \pm 2.01 \times 10^{-3}$
3.34	$0.906 \pm 1.92 \times 10^{-3}$	$0.901 \pm 1.48 \times 10^{-3}$	$1.228 \pm 3.49 \times 10^{-3}$	$1.250 \pm 2.35 \times 10^{-3}$
3.96	$0.918 \pm 2.28 \times 10^{-3}$	$0.908 \pm 1.92 \times 10^{-3}$	$1.177 \pm 2.35 \times 10^{-3}$	$1.228 \pm 2.33 \times 10^{-3}$

Table 4 The λ of compressed specimens under paraffin lubrication condition

Amplitude (μm)	λt	λb	$\lambda' t$	$\lambda' b$
0	$0.906 \pm 1.87 \times 10^{-3}$	$0.906 \pm 1.14 \times 10^{-3}$	$1.126 \pm 1.92 \times 10^{-3}$	$1.126 \pm 1.99 \times 10^{-3}$
3.34	$0.933 \pm 2.17 \times 10^{-3}$	$0.908 \pm 2.68 \times 10^{-3}$	$1.100 \pm 2.05 \times 10^{-3}$	$1.115 \pm 2.03 \times 10^{-3}$
3.96	$0.943 \pm 2.55 \times 10^{-3}$	$0.925 \pm 2.95 \times 10^{-3}$	$1.049 \pm 3.37 \times 10^{-4}$	$1.084 \pm 2.66 \times 10^{-3}$

Table 5 The λ of compressed specimens under lithium grease lubrication condition

Amplitude (μm)	λt	λb	$\lambda' t$	$\lambda' b$
0	$0.968 \pm 2.86 \times 10^{-3}$	$0.968 \pm 3.03 \times 10^{-3}$	$0.887 \pm 1.78 \times 10^{-3}$	$0.887 \pm 4.12 \times 10^{-3}$
3.34	$0.974 \pm 2.49 \times 10^{-3}$	$0.968 \pm 2.88 \times 10^{-3}$	$0.968 \pm 3.21 \times 10^{-3}$	$0.916 \pm 2.56 \times 10^{-3}$
3.96	$0.976 \pm 2.01 \times 10^{-3}$	$0.974 \pm 1.58 \times 10^{-3}$	$0.992 \pm 1.69 \times 10^{-3}$	$0.941 \pm 1.76 \times 10^{-3}$

Fig. 3, where R_n is the radius of the neutral layer and R_o, R_i, and H are the external radius, internal radius, and height of the original specimen, respectively. r_o, r_i, and h are the external radius, internal radius, and height of the deformed specimen. Varying with process parameters, the radius of the neutral layer can be larger or smaller than the internal radius [24].

The theoretical relationship among the radius of the neutral layer R_n, the friction factor m, and the original size can be obtained based on the energy method.

When $R_n = R_i$, the friction factor on the specimen/tool interface reaches the critical value m_f which can be expressed as Eq. (1).

$$m_f = \frac{1}{2(1-R_i/R_o)R_o/H} \ln\left[\frac{3(R_o/R_i)^2}{1+\sqrt{1+3(R_o/R_i)^4}}\right] \quad (1)$$

Actually, R_n and m are not constants in the course of ring upsetting, if the deformation of ring upsetting is divided into lots of identical small deformations and assumed that each small deformation is under the action of a predetermined friction coefficient m. By the time, R_n can be regarded as invariable.

When $m \le m_f$ ($R_n \le R_i$), the R_n is calculated by Eq. (2).

$$R_n = \left\{\frac{\sqrt{3}}{2}\frac{1-(R_i/R_o)^4x^2}{\left[x(x-1)\left(1-(R_i/R_o)^4x\right)\right]^{1/2}}\right\}^{1/2} R_o \quad (2)$$

where

$$x = \left\{\frac{R_o}{R_i}\exp\left[-m\frac{R_o}{H}\left(1-\frac{R_i}{R_o}\right)\right]\right\}^2 \quad (3)$$

When $m > m_f$ ($R_i < R_n < R_o$), the R_n is determined by Eq. (4).

$$R_n = \frac{2\sqrt{3}m^{R_o/H}}{(R_o/R_i)^2-1}\left\{\left[1+\frac{(1+R_i/R_o)\left[(R_o/R_i)^2-1\right]}{2\sqrt{3}m^{R_o/H}}\right]^{1/2}-1\right\}R_o \quad (4)$$

When the upsetting reduction in height is h, the internal radius r_o and external radius r_i can be calculated based on the volume constancy condition.

$$r_i = \left[\frac{R_n^2 h-\left(R_n^2-R_i^2\right)H}{h}\right]^{1/2} \quad (5)$$

Table 6 The λ of compressed specimens under PTFE film lubrication condition

Amplitude (μm)	λt	λb	$\lambda' t$	$\lambda' b$
0	$0.988 \pm 2.12 \times 10^{-3}$	$0.988 \pm 2.49 \times 10^{-3}$	$0.986 \pm 2.36 \times 10^{-3}$	$0.988 \pm 3.01 \times 10^{-3}$
3.34	$0.996 \pm 1.87 \times 10^{-3}$	$0.990 \pm 1.22 \times 10^{-3}$	$0.996 \pm 1.98 \times 10^{-3}$	$0.988 \pm 2.03 \times 10^{-3}$
3.96	$0.998 \pm 1.64 \times 10^{-3}$	$0.994 \pm 1.30 \times 10^{-3}$	$0.998 \pm 2.11 \times 10^{-3}$	$0.990 \pm 1.65 \times 10^{-3}$

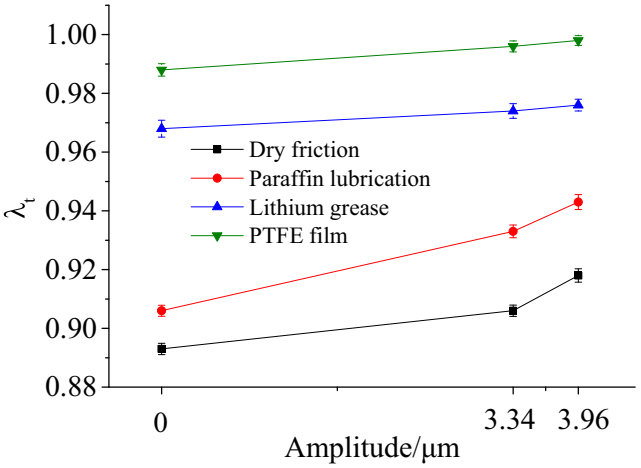

Fig. 8 The change of λ_t under different lubrication conditions

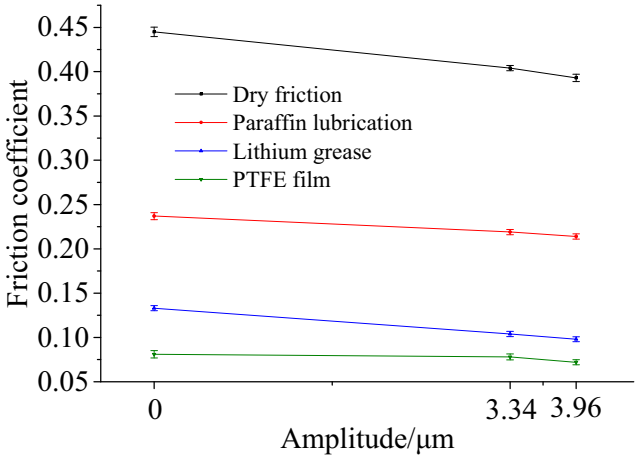

Fig. 9 The variation of friction coefficient with the change of ultrasonic amplitude under the four kinds of lubrication conditions

$$r_o = \left[\frac{H\left(R_o^2 - R_i^2\right)}{h} + r_i^2\right]^{1/2} \tag{6}$$

The size of the specimen after the first deformation is regarded as the original size of the second deformation, and then, the ring size after the second deformation can be calculated according to Eqs. (5) and (6). So repeatedly, a series of m, h, and r_i can be obtained. The theoretical calibrating curves between the internal radius and the upsetting reduction in height under different friction factors are gotten from these data, as shown in Fig. 4.

According to the internal radius and height of the deformed ring, the associated friction factor m can be directly derived from the theoretical calibrating curves. The friction coefficient μ can be obtained based on the relationship between μ and m in Eq. (7).

$$\mu = m/\sqrt{3} \tag{7}$$

3 Experimental study on the surface effect during ultrasonic vibration-assisted ring upsetting

Figure 5 shows the stress-strain curves of upsetting under the dry friction condition. Obviously, after applying the ultrasonic vibration, the material produces softening and the stress decreases immediately at the moment of applying ultrasonic vibration. Siddiq and Sayed [25, 26] indicated that ultrasonic energy was preferentially absorbed in highly localized regions such as dislocations, voids, and grain boundaries. An additional stress field is induced by the ultrasonic vibration, which makes the dislocation movement be easy and accelerate it. Consequently, the material is easily deformed and the flow stress decreases.

The decreasing range of the stress is related to the vibration amplitude. When the amplitude is 3.34 μm, the stress decreases by 3.03 MPa at the time of applying ultrasonic, the decreasing rate is 14.26% compared with the stress under static upsetting condition. While the amplitude is 3.96 μm, the stress decreases by 3.38 MPa, the decreasing rate is 15.45%. And the stress under the vibration is always lower than the static stress. Due to the limited experimental condition, only two kinds of small amplitudes were applied in the upsetting process. The amplitude ratio $\lambda_A = A_2 / A_1$ is only 1.18, so the ratio of stress drops $\lambda_{\Delta\sigma} = \Delta\sigma_2 / \Delta\sigma_1$ under different amplitudes is smaller, 1.12. Where the amplitudes A_1 = 3.34 μm and A_2 = 3.96 μm, $\Delta\sigma_1$ and $\Delta\sigma_2$ are the stress drop at the time of applying the ultrasonic vibration of which amplitude are 3.34 and 3.96 μm, respectively. When the upsetting reduction in height is 3 mm, the stresses of specimens D1, D2, and D3 are 129.12, 124.36, and 124.19 MPa, respectively.

Figure 6 shows the stress-strain curves of static upsetting under different lubrication conditions. It can be found that the upsetting loads under the lubrication conditions of paraffin, lithium grease, and PTFE film lubrications are slightly lower than those under the dry friction condition; the stress

Table 7 The friction coefficient under different lubricating and ultrasonic vibration conditions

Amplitude (μm)	Dry friction	Paraffin lubrication	Lithium grease lubrication	PTFE film lubrication
0	$0.445 \pm 5.35 \times 10^{-3}$	$0.237 \pm 3.96 \times 10^{-3}$	$0.133 \pm 2.87 \times 10^{-3}$	$0.081 \pm 4.24 \times 10^{-3}$
3.34	$0.404 \pm 2.96 \times 10^{-3}$	$0.219 \pm 2.98 \times 10^{-3}$	$0.104 \pm 3.03 \times 10^{-3}$	$0.078 \pm 3.35 \times 10^{-3}$
3.96	$0.393 \pm 4.11 \times 10^{-3}$	$0.214 \pm 3.06 \times 10^{-3}$	$0.098 \pm 2.89 \times 10^{-3}$	$0.072 \pm 2.88 \times 10^{-3}$

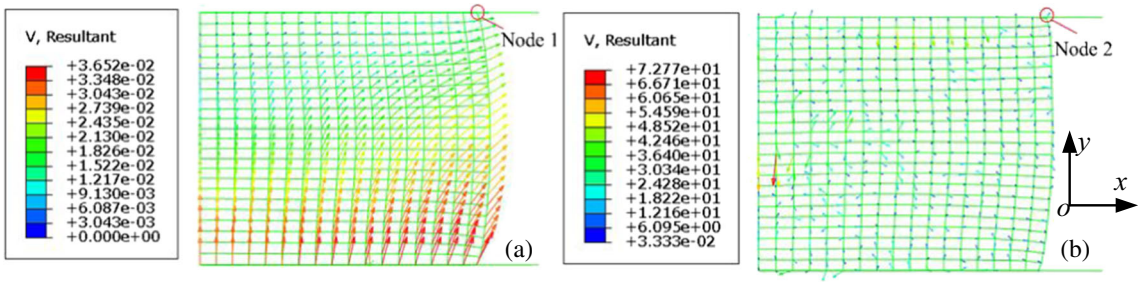

Fig. 10 Distributions of the velocity field at the same reduction in height: **a** upsetting without ultrasonic and **b** ultrasonic vibration-assisted upsetting (mm s^{-1})

decreasing rate is 5.37, 6.28, and 10.89%, respectively. Compared to the upsetting load under the dry friction condition, the decreasing rate of the upsetting load is larger than 14% when applying the ultrasonic vibration. The average decreasing rate of the upsetting load is 7.51% under different lubrication conditions. The result shows that the upsetting load cannot lower significantly only by improving the lubrication condition. The influence of the lubrication condition on ring upsetting is lower than that of ultrasonic vibration.

The beneficial impacts of the ultrasonic vibration on metal forming processes mainly include surface and volume effects. Generally, the volume effect causes the material softening. According to [13, 17, 27, 28], there were three viewpoints about the material softening induced the volume effect, they are (1) dislocations absorbing energy through resonance and overcoming slip obstacles, (2) the internal friction effect, and (3) the superposition of steady stress and alternating stress. Nevill and Brotzen [29] attributed the reduction of the flow stress to the superposition of steady stress and the alternation of stress, and proposed the stress superposition mechanism. Kempe and Kroner [30] proposed three mechanisms by which dislocations may absorb energy from vibrations: they are (1) a resonance mechanism, (2) a relaxation mechanism, and (3) a mechanism of simple hysteresis. The surface effect can reduce the friction coefficient on the tool/workpiece interface and improve the lubrication condition and the surface quality of the workpiece.

3.1 Effect of ultrasonic vibration on interface friction coefficient between the tool/specimen interface

During upsetting, the friction status on the tool/specimen interface has a significant impact on upsetting load and the deformed shape. The material that is near the contact surface is restricted due to the existence of the interface friction and the deformed specimen gradually becomes drum-shaped. Thus, the drum ratio of the specimen is a sign to evaluate the size of the friction coefficient on the tool/specimen interface, under different ultrasonic vibration and friction conditions, the deformation process, and upsetting characteristics. In order to quantificationally describe the geometrical shape of the deformed specimen, area ratios λt, λb, $\lambda' t$, and $\lambda' b$ are defined.

$$\lambda_t = S_t/S_m = D_t^2/D_m^2 \lambda_b = S_b/S_m = D_b^2/D_m^2 \tag{8}$$

$$\lambda_t' = s_t/s_m = d_t^2/d_m^2 \lambda_b' = s_b/s_m = d_b^2/d_m^2 \tag{9}$$

where D and S are the external diameter and the area of the compressed specimen, respectively. d and s are the internal diameter and the area of the compressed specimen, respectively. Subscripts t, m, and b represent the top surface which

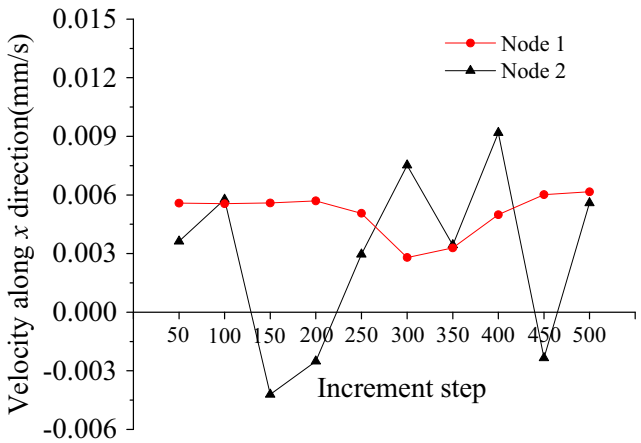

Fig. 11 Variation of velocity along x direction of nodes 1 and 2 with increment step

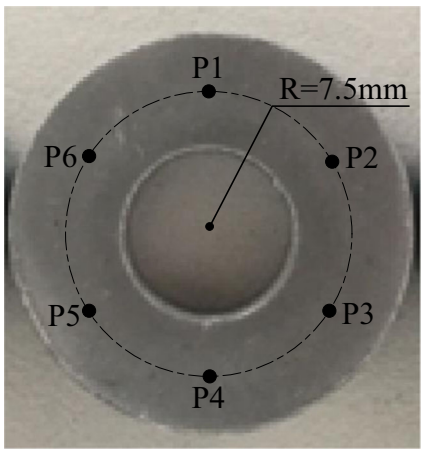

Fig. 12 The distribution of six measurement points

Table 8 The surface hardness under different lubrication conditions (HRB)

	Original specimen	D1	D3	PA4	PA6	L7	L9
Top surface	78.93	90.35	90.44	91.7	92.7	92	90.1
Bottom surface		89.88	87.24	92	90.75	91.7	89.2
Hardness difference	–	0.47 ± 0.036	3.2 ± 0.042	0.3 ± 0.029	2.9 ± 0.04	0.3 ± 0.041	0.9 ± 0.027

contacts with the ultrasonic tool head, middle surface, and the bottom surface, respectively. The characteristic dimensions of compressed specimens are given in Fig. 7. Obviously, the area ratio approaches to 1 when the difference between the middle surface and the bottom surface or the top surface is getting smaller and smaller. It also means the friction coefficient on the tool/specimen interface approaches 0. Figure 7b shows the cross-sectional profiles of the specimens D1, D2, D3, L7, L8, and L9 when the reduction in height is 3 mm. The characteristic dimensions are listed in Fig. 7.

The friction coefficients are relatively large under the dry friction and paraffin lubrication. Thus, the neutral layer is within the ring, the metals within the neutral layer flow inwards, and the metals outside the neutral layer flow outwards. On the contrary, the friction coefficient is relatively small under the lithium grease lubrication and PTFE film lubrication conditions. Therefore, the diameter of neutral layer is smaller than the internal diameter of the ring, all of metals flow outwards. Tables 3, 4, 5, and 6 show the area ratios of the compressed specimens for static upsetting and vibration upsetting under the four different kinds of lubrication conditions.

All values of λ under the four lubrication conditions are less than 1. With the improvement of the lubrication effect, the area ratio approaches to 1. The area ratio increases and is closer to 1 with the increase of the vibration amplitude under the same lubrication condition, as shown in Fig. 8. Clearly, the ultrasonic vibration improves the friction condition on the tool/specimen interface. The values of λ' are greater than 1 under dry friction and paraffin lubrication conditions and are less than 1 under lithium grease and PTFE film lubrications. For a bigger amplitude, the area ratio is further closer to 1. The area ratios of the top and bottom surfaces of the specimens without the ultrasonic vibration are almost identical. Introducing the effect of ultrasonic vibration, the area ratio λt of the top surface is bigger than λb of the bottom surface. It shows that the anti-friction effect on the top surface is better than that on the bottom surface.

Thus, different lubrication and ultrasonic vibration conditions can cause the change of the friction coefficient on tool/specimen interface and, then, impact greatly on the upsetting deformation. The drum degree of the upset specimen changes. Table 7 shows the friction coefficient under different lubrication and ultrasonic vibration conditions. Compared to specimen D1, the friction coefficients of specimens D2 and D3 decrease by 0.041 and 0.052 under the dry friction, i.e., the decreasing range is 9.21 and 11.69%, respectively. Compared to specimen PA4, the friction coefficients of specimens PA5 and PA6 decrease by 0.018 and 0.023 under paraffin lubrication, i.e., the decreasing range is 7.59 and 9.7%. Compared to specimen L7, the friction coefficients of specimens L8 and L9 decrease by 0.029 and 0.035 under lithium grease lubrication, i.e., the decreasing range is 21.8 and 26.32%. Compared to specimen PT10, the friction coefficient of specimens PT11 and PT12 decrease by 0.003 and 0.009 under PTFE film lubrication, i.e., the decreasing range is 3.7 and 11.1%. Figure 9 shows the variation of friction coefficient with the ultrasonic amplitude under the four kinds of lubrication conditions. The friction coefficient decreases with the increasing amplitude under different friction conditions. The anti-friction effect of the ultrasonic vibration is best under lithium grease lubrication condition.

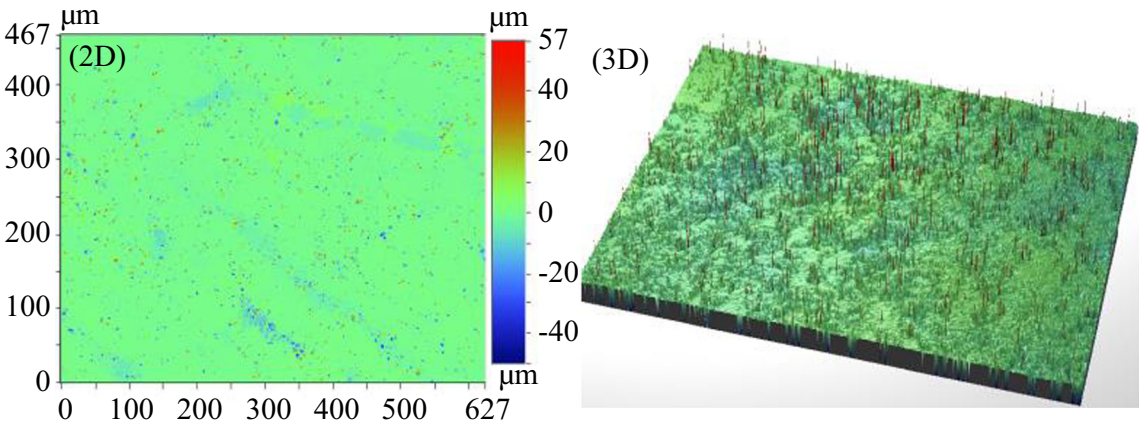

Fig. 13 Local 2D and 3D surface topography images of the initial specimen

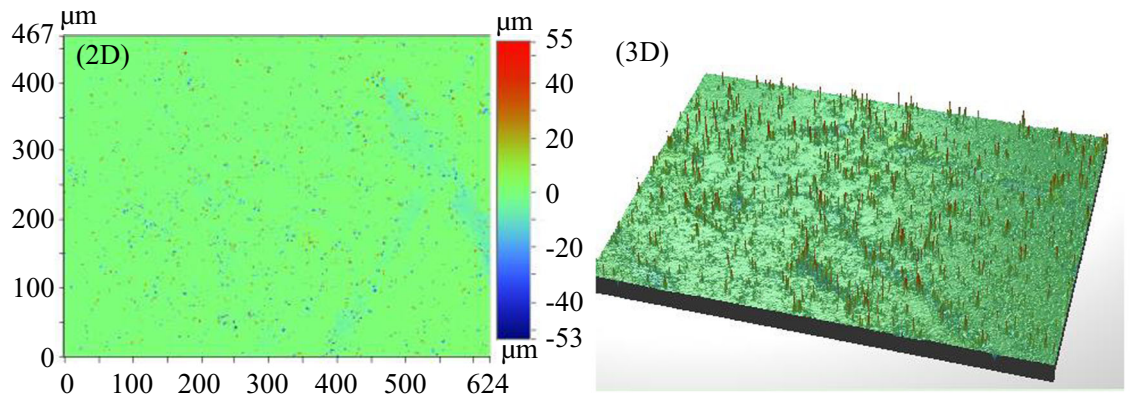

(a) Specimen D1

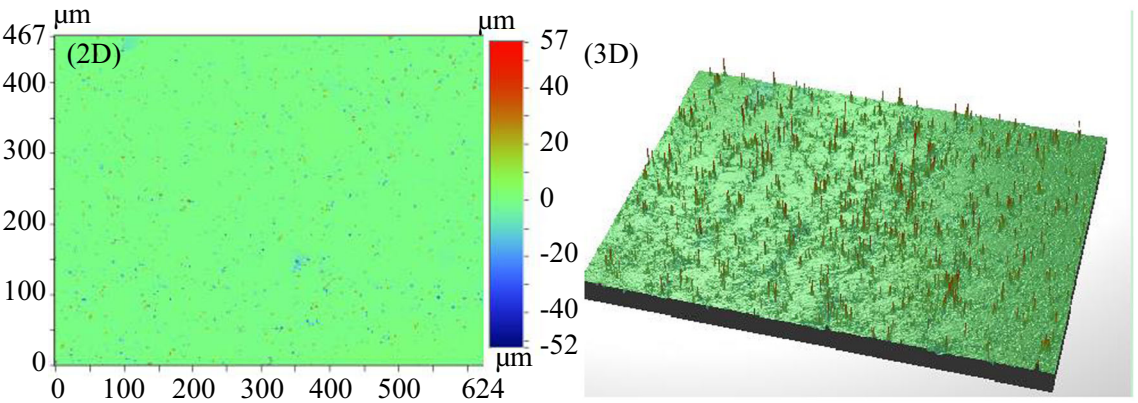

(b) Specimen D2

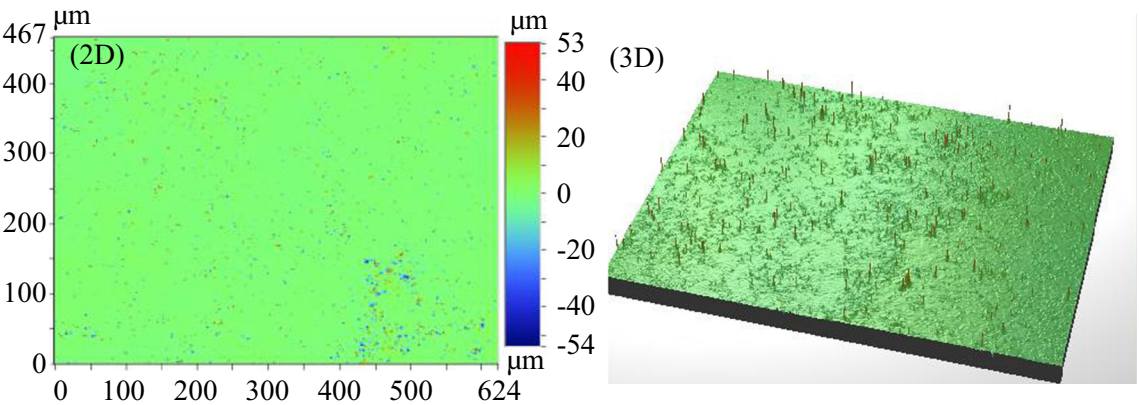

(c) Specimen D3

Fig. 14 Local 2D and 3D surface topography images of specimens D1 (**a**), D2 (**b**), and D3 (**c**)

Obviously, after applying the ultrasonic vibration, the friction coefficient on the tool/specimen interface decreases. The ultrasonic vibration produces a similar effect like the lubrication. It means a stronger surface effect occurs. Siegert and Mock [31] pointed out applying the ultrasonic vibration led to frequent separations between the tool and specimen. It is hard to investigate the flow of material in the upsetting process, so the upsetting

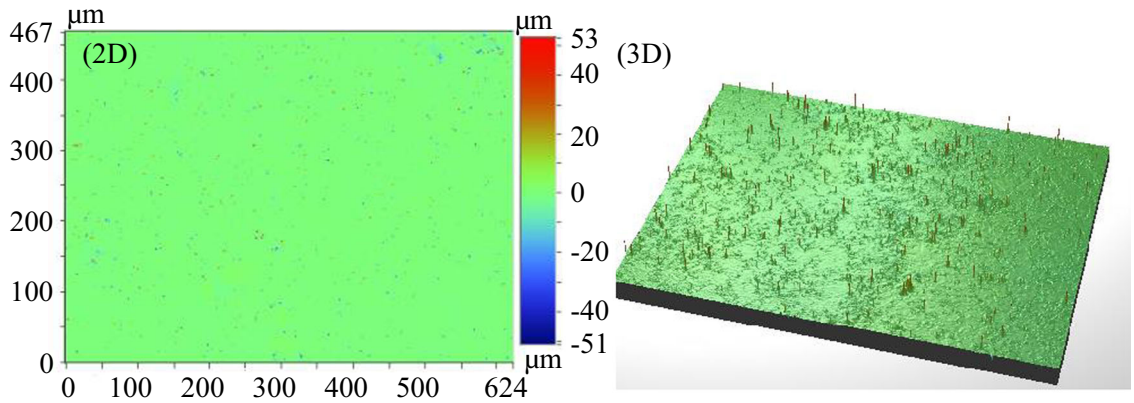

(a) Specimen PA4

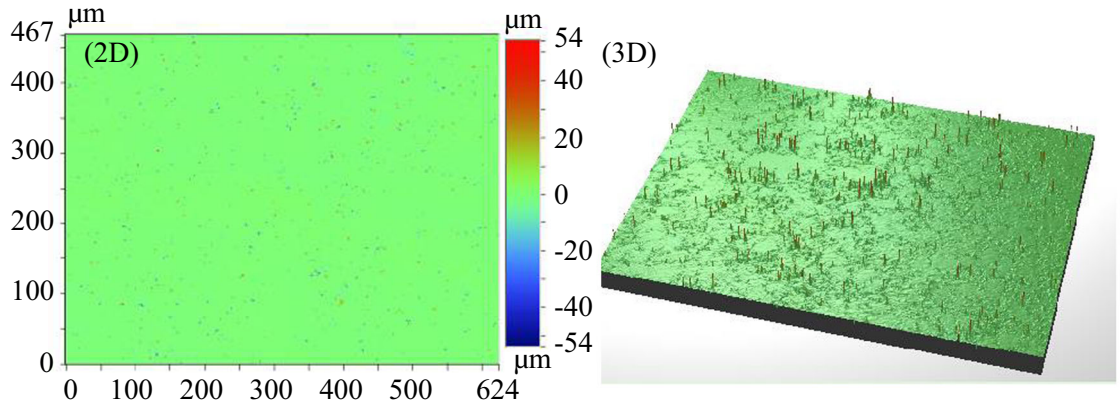

(b) Specimen PA5

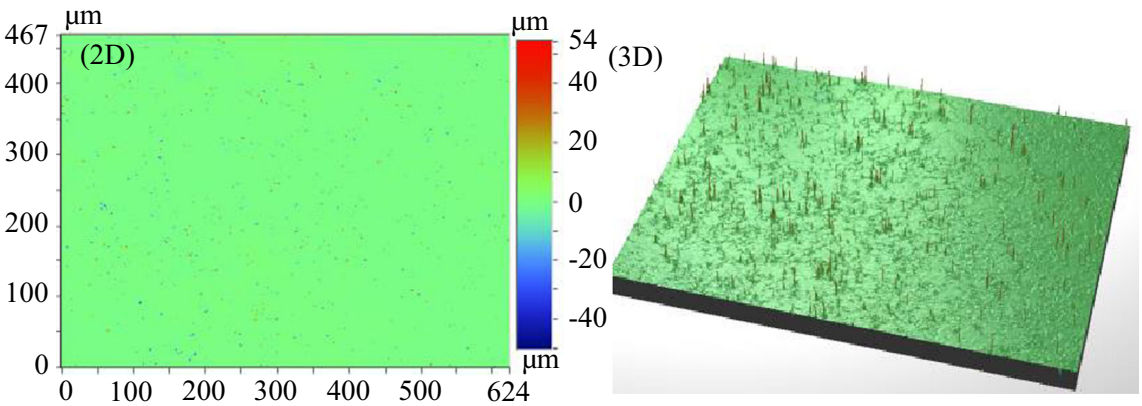

(c) Specimen PA6

Fig. 15 Local 2D and 3D surface topography images of specimens PA4 (**a**), PA5 (**b**), and PA6 (**c**)

process was analyzed with the aid of the finite element software ABAQUS [18]. Figure 10 shows the velocity vector fields at some point. In conventional upsetting process, the flow direction of material in horizontal is consistent. However, the flow of material is no longer in the same direction under the effect of ultrasonic

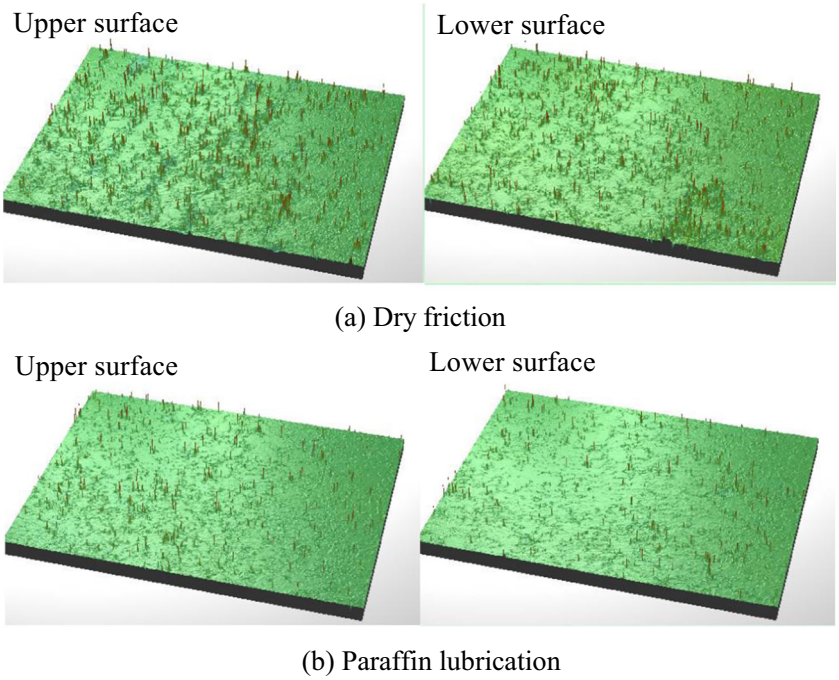

Fig. 16 Local 3D surface topography images of specimens D3 and PA6. **a** Dry friction. **b** Paraffin lubrication

vibration. The nodes 1 and 2 shown in Fig. 10 are selected to analyze the change of flow direction of material over time. Figure 11 shows the change of horizontal velocity of nodes 1 and 2 over time. Under the effect of ultrasonic vibration, the direction of the relative velocity vector between the tool and the specimen along the horizontal direction no longer keeps invariably, but changes frequently. On the other hand, applying the ultrasonic vibration makes the flow stress decreased, and the contact pressure on the tool/specimen interface also decreases. Both the change in relative velocity vector and decrease in contact pressure on the tool/specimen interface are helpful for the decrease of the friction coefficient on the tool/specimen interface.

Besides the change of the friction coefficient, the surface effect also has a dramatic influence on surface quality, including surface hardness, surface roughness, and surface topography.

3.2 Effect of the ultrasonic vibration on surface hardness

The surface Rockwell hardness of specimens was measured by a HR-150A Rockwell hardness tester. The indenter diameter is 1.588 mm and the initial and final loads are 98.07 and 980.7 N, respectively. Uniformly distributed six points surrounding the centers of the top and bottom surfaces are defined to measure and average the surface hardness. The distribution of six measurement points is shown in Fig. 12. Table 8 shows the hardness of the top and bottom surfaces of the deformed specimen under different lubrication conditions.

Compared with the initial specimen, different hardening occurs on the top and bottom surfaces of all deformed specimens. Under different lubrication conditions, the hardness of the top and bottom surfaces of the specimens without the ultrasonic vibration is almost identical. Bagherzadeh et al. [32] attributed the increase of microhardness in the samples processed using ultrasonic propagation to more grain refinement as a result of dislocation density rise and subgrain boundaries formation. After applying the ultrasonic vibration, the hardening degree of the top surface which directly contacts with the ultrasonic tool head is apparently higher than that of the bottom surface. When the amplitude is 3.96 μm, the hardness value of the top surface is 3.2 HRB higher than the bottom surface hardness under dry friction; the changing range is 3.67%. The hardness values of the top surface are 2.9 HRB higher than the bottom surface hardness under paraffin lubrication condition; the changing range is 3.25%. The hardness difference between the top and bottom surfaces declines a little under the lithium grease lubrication condition. Mousavi et al. [33] also found that ultrasonic-assisted forming could improve surface condition. However, with the increase in amplitude, surface quality can be no longer improved obviously.

3.3 Effect of the ultrasonic vibration on surface roughness and topography

A Veeco NT9300 non-contact optical surface profilometer was employed to measure the two-dimensional (2D) and three-dimensional (3D) surface topography images and different surface roughness of initial and deformed specimens. The surface roughness is characterized by the arithmetic average

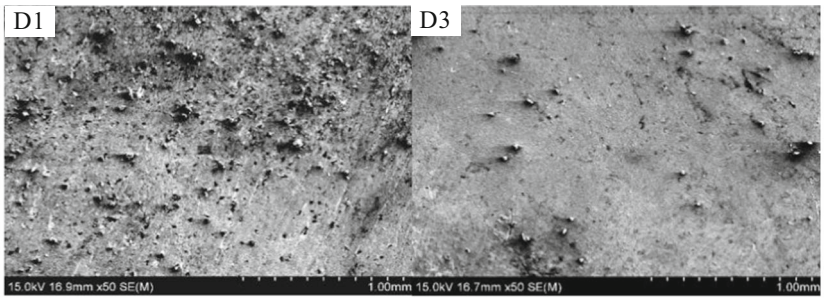

(a) Dry friction

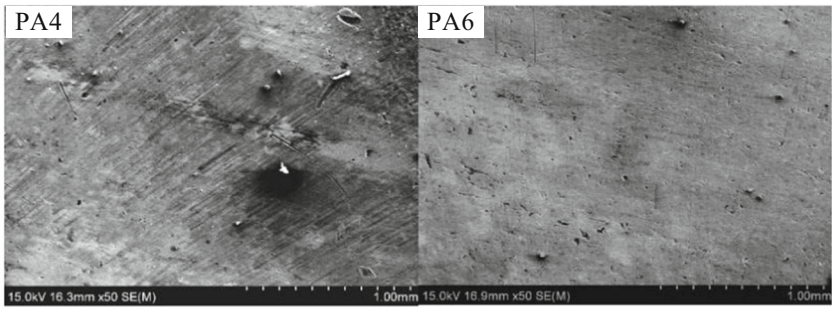

(b) Paraffin lubrication

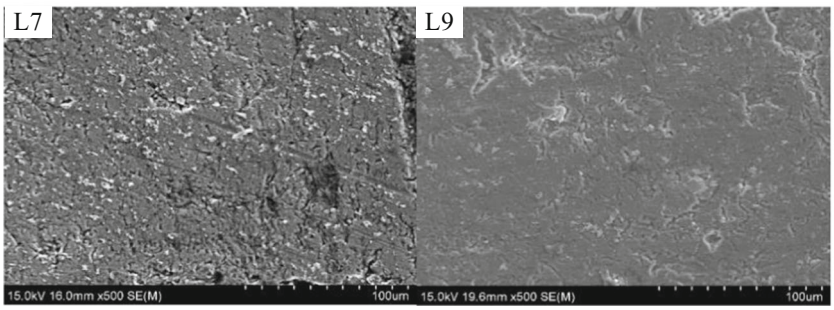

(c) Lithium grease lubrication

Fig. 17 The top surface topographies of the specimens D1, D3, PA4, PA6, L7, and L9 (× 50). **a** Dry friction. **b** Paraffin lubrication. **c** Lithium grease lubrication

deviation (Ra). The measurement area is about 624 × 467 μm and the magnification times is 10. The roughness was measured for three times at different positions and averaged as the final result. Figure 13 shows the local 2D and 3D surface topography images of the initial specimen. The average surface roughness Ra is 2.39 μm.

Figure 14 shows the local 2D and 3D surface topography images of specimens D1, D2, and D3 under the dry lubrication condition. After upsetting, the surface roughness Ra of specimen 1 is 1.56 μm. After applying the ultrasonic vibration, the Ra values of the specimens D2 and D3 are 1.37 and 1.3 μm, which are 12.18 and 16.67% less than the specimen D1, respectively. It is obvious that the ultrasonic vibration can dramatically decrease the sharp ridges on the specimen surface and improve the surface roughness, so the surface becomes smooth. It means the ultrasonic vibration is beneficial to the surface material flow and makes the surface material flow uniform.

Figure 15 shows local 2D and 3D surface topography images of specimens PA4, PA5, and PA6 under the paraffin lubrication condition. The surface roughness Ra of the specimen PA4 without the ultrasonic vibration is 905.88 nm, while the Ra values of specimens PA4 and PA5 that the related amplitudes are 3.34 and 3.96 μm decrease to 732.84 and 622.5 nm. Compared to the specimen PA4, the decrease ranges are 19.1 and 31.28%, respectively. Therefore, under the paraffin lubrication condition, the changing trend of Ra is similar to that under the dry friction condition, which means that the roughness of the top and bottom surfaces improves greatly and decreases with the increase of the amplitude.

Figure 16 gives local 3D surface topography images of the top and bottom surfaces of specimens D3 and PA6. The average Ra values of the top and bottom surfaces under the dry friction are 1.3 and 1.48 μm, respectively. Meanwhile, Ra values of the top and bottom surfaces for the paraffin lubrication 622.5 and 816.37 nm. Obviously, the top and bottom

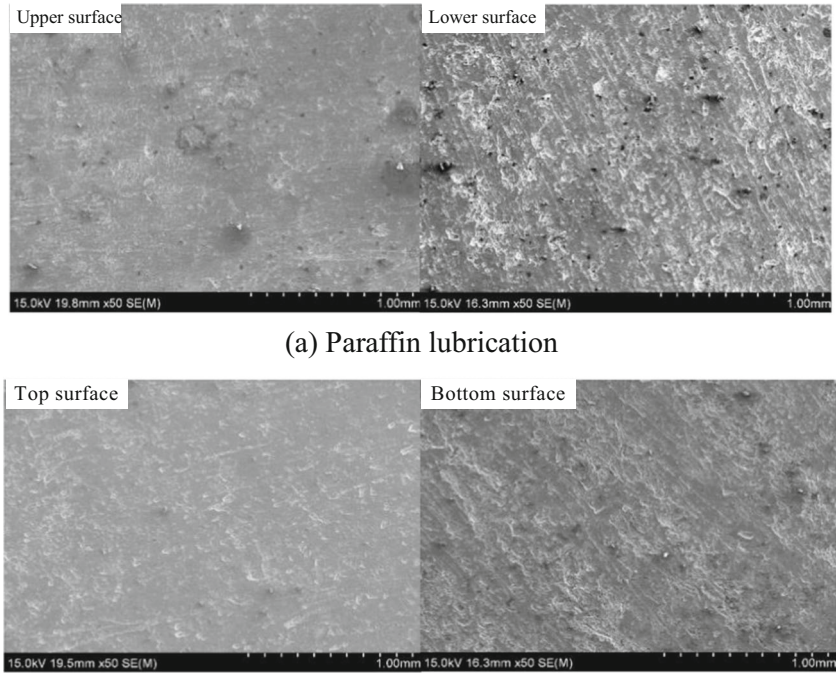

(a) Paraffin lubrication

(b) Lithium grease lubrication

Fig. 18 Topographies of the top and bottom surfaces of specimens PA6 and L9 (× 50). **a** Paraffin lubrication. **b** Lithium grease lubrication

surface quality under the paraffin lubrication is better than that of the dry friction. Especially, under the ultrasonic vibration, the sharp ridges of the top surface are less than those of the bottom surface.

Compared with the dry friction, using of the paraffin lubrication during upsetting improves the plastic flow of materials and reduces the surface roughness. After applying the ultrasonic vibration, the surface roughness of the specimen also decreases, which indicates that the ultrasonic vibration improves the friction status of the tool/specimen interface. However, the improvement of the top surface is better than that of the bottom surface because the top surface contacts directly with the ultrasonic tool head. On the contrary, because the energy loss occurs when the ultrasonic vibration spreads in the specimen, the impact of the ultrasonic vibration on the bottom surface is apparently weaker than the that on top surface.

Figure 17 shows the top surface topographies of the specimens D1, D3, PA4, PA6, L7, and L9. Clearly, the surface of the deformed specimens without ultrasonic vibration is uneven and the surface quality is poor because there are so many micro-bulges and pits on the specimen surface, particularly under dry friction. The surface of the deformed specimens becomes smooth after applying the ultrasonic vibration and different lubricants, and the density of micro-bulges and pits decreases. It further shows that the ultrasonic vibration plays a similar role of the lubricant, i.e., can reduce the surface friction and improve the surface quality.

Figure 18 shows the topographies of the top and bottom surfaces of specimens PA6 and L9. It can be seen that the top surface quality is better than the bottom surface quality even though the lubrication conditions of the top and bottom surfaces are identical during the upsetting process. The top surface contacts directly with the ultrasonic tool head; the ultrasonic energy is high. The ultrasonic energy loss occurs during spreading in the specimen, so the ultrasonic energy of the bottom surface is relatively weak and its surface quality is lower than that of the top surface. Lou et al. [34] also indicated high-frequency friction inevitably resulted in improving surface quality and reducing the friction coefficient.

After applying the ultrasonic vibration, the decreasing range of the friction coefficient under the lithium grease lubrication condition is higher than that under the paraffin lubrication condition. The different lubrication mediums have different ability to reflect and absorb the ultrasonic energy. More ultrasonic energy can act on the specimen under the lithium grease lubrication condition and the lithium grease can better fill the surface pits under the effect of ultrasonic vibration; thus, anti-friction effect of the lithium grease is better than on paraffin.

To some extent, the surface qualities of specimens are improved under the effect of ultrasonic vibration; this is mainly because the surface effect induced by the ultrasonic vibration. After applying the ultrasonic vibration, the instantaneous separation of the specimen with the vibration tool head occurs constantly due to the ultrasonic vibration, and the direction of the friction force on the specimen/tool interface changes

continuously, so that the friction force contributes to deformation in part time of the vibration period. Furthermore, the micro-bulges and pits on the specimen surface reduce under the effect of the ultrasonic vibration, which diminishes the probability of occlusion with the micro-bulges and pits of the tool. The shear resistance to shear off the occlusal micro-bulges and pits reduces. Meanwhile, during the experiment, the temperatures of both the ultrasonic tool head and the specimen rise under the effect of the ultrasonic vibration. This shows that the ultrasonic vibration can induce the local heating effect and reduce the local soldering. The lubricant is to easily fill into the contact surface so that the ultrasonic vibration also improves the surface lubrication condition and makes the friction coefficient decrease. Thus, the decrease of friction force and the effect of local thermal effect promote the plastic flow of the material, and the surface quality is improved.

Under the effect of the ultrasonic vibration, the forming quality of the top surface is better than that of the bottom surface. It shows that the surface effect on the top surface is stronger than that on the bottom surface. In the process of vibration upsetting, the top surface contacts directly with the vibration tool head, so the effect of ultrasonic energy on the top surface is higher. The ultrasonic energy loss occurs during spreading in the specimen, so the ultrasonic energy of the bottom surface is relatively weaker. Consequently, the surface quality, roughness, hardness, and anti-friction effect on the top surface is better than those on the bottom surface.

4 Conclusions

The ultrasonic vibration-assisted 6063 aluminum alloy ring upsetting was performed. The impact of ultrasonic vibration on the variation of friction coefficient under the different lubricant conditions, as well as the influence of ultrasonic vibration on surface topography, surface hardness, and surface roughness, was studied. The principal conclusions are as follows:

(1) The ultrasonic vibration makes the material produce softening. The larger the vibration amplitude is, the more obvious the softening effect is. The upsetting load cannot decrease significantly only by improving the lubrication condition. Under the processing parameters mentioned in this paper, the influence of the lubrication condition on ring upsetting is lower than that of ultrasonic vibration.

(2) The friction coefficient on the specimen/tool interface reduces under the effect of ultrasonic vibration, and the friction coefficient decreases with the increase of the vibration amplitude. The effect of the ultrasonic vibration on reducing the friction coefficient is different under different lubrication conditions. The anti-friction effect of the ultrasonic vibration is stronger under grease lubrication condition.

(3) Under the effect of the ultrasonic vibration, the surface hardness increases and the surface roughness reduces. The ultrasonic vibration improves the surface quality effectively. The larger the vibration amplitude is, the better the effect is. The quality of the top surface that contact directly with the vibration tool head is better than that of the bottom surface. The ultrasonic energy loss occurs during spreading in the specimen, so the ultrasonic energy of bottom surface is relatively weak. Consequently, the surface quality, roughness, hardness, and anti-friction effect on the top surface is better than those of the bottom surface.

Funding information The research work was supported by the National Natural Science Foundation of China (Approval Nos. 51375269, 51675307).

References

1. Yang C, Shan X, Xie T (2016) Titanium wire drawing with longitudinal-torsional composite ultrasonic vibration. Int J Adv Manuf Technol 83(1–4):645–655
2. Kim J, Lee E (1996) A study of ultrasonic vibration cutting of carbon fibre reinforced plastics. Int J Adv Manuf Technol 12(2): 78–86. https://doi.org/10.1007/BF01178947
3. Ahmadi F, Farzin M, Meratian M, Loeian SM, Forouzan MR (2015) Improvement of ECAP process by imposing ultrasonic vibrations. Int J Adv Manuf Technol 79(1–4):503–512
4. Bunget C, Ngaile G (2011) Influence of ultrasonic vibration on micro-extrusion. Ultrasonics 51(5):606–616. https://doi.org/10.1016/j.ultras.2011.01.001
5. Jimma T, Kasuga Y, Iwaki N, Miyazawa O, Mori E, Ito K, Hatano H (1998) An application of ultrasonic vibration to the deep drawing process. J Mater Process Tech 80:406–412
6. Ashida Y, Aoyama H (2007) Press forming using ultrasonic vibration. J Mater Process Tech 187:118–122
7. Schey JA (1984) Tribology in metalworking: friction, lubrication, and wear. J Appl Metalwork 3(2):173–173. https://doi.org/10.1007/BF02833697
8. Blaha F, Langenecker B (1955) Elongation of zinc monocrystals under ultrasonic action. Die Natur Wissenschafen 42(20):556. https://doi.org/10.1007/BF00623773
9. Langenecker B (1966) Effects of ultrasound on deformation characteristics of metals. IEEE Trans Son Ultrason 13(1):1–8. https://doi.org/10.1109/T-SU.1966.29367
10. Murakawa M, Jin M, Kaewtatip P (1999) Utility of ultrasonic vibration applied to metal-forming processes. Proceedings of the 6th international conference on technology of plasticity, Nuremberg: 19–24
11. Huang H, Pequegnat A, Chang BH, Mayer M, Du D, Zhou Y (2009) Influence of superimposed ultrasound on deformability of Cu. J Appl Phys 106(11):113514
12. Hayashi M, Jin M, Thipprakmas S, Murakawa M, Hung J, Tsai Y, Hung C (2003) Simulation of ultrasonic-vibration drawing using the finite element method (FEM). J Mater Process Technol 140(1):30–35

13. Daud Y, Lucas M, Huang Z (2006) Superimposed ultrasonic oscillations in compression tests of aluminium. Ultrasonics 44:e511–e515
14. Siegert K, Ulmer J (2001) Superimposing ultrasonic waves on the dies in tube and wire drawing. J Eng Mater Technol ASME 123(4): 517–523. https://doi.org/10.1115/1.1397779
15. Pohlman R, Lehfeldt E (1966) Influence of ultrasonic vibration on metallic friction. Ultrasonics 4(4):178–185. https://doi.org/10.1016/0041-624X(66)90244-7
16. Dawson GR, Winsper CE, Sansome DH (1996) Application of high and low frequency scillations to the plastic deformation of metal. Metal Form 231(8):234–238
17. Huang Z, Lucas M, Adams MJ (2002) Influence of ultrasonics on upsetting of a model paste. Ultrasonics 40(1):43–48
18. Daud Y, Lucas M, Huang Z (2007) Modelling the effects of superimposed ultrasonic vibrations on tension and compression tests of aluminium. J Mater Process Tech 186(1):179–190
19. Abdul Aziz S, Lucas M (2010) The effect of ultrasonic excitation in metal forming tests. Appl Mech Mater 24:311–316 Trans Tech Publ
20. Zhuang X, Wang J, Zheng H, Zhen Z (2015) Forming mechanism of ultrasonic vibration assisted compression. Trans Nonferrous Metals Soc China 25(7):2352–2360
21. Kobayashi S (1970) Deformation characteristics and ductile fracture of 1040 steel in simple upsetting of solid cylinders and rings. J Ind Eng Int 92(2):391–398
22. Kobayashi S, Kobayashi S, Oh S, Altan T (1989) Metal forming and the finite-element method. Oxford University Press on Demand, Oxford
23. Male A T (2002) Friction measurement using the ring compression test. Proceedings of the Seventh ICTP Conference 1: 321–326
24. Xu S, Zhao J (2002) Mathematical expression of calibration curves for measuring friction factor by ring upsetting. J Plast Eng 9:25–27
25. Siddiq A, Sayed TE (2011) Acoustic softening in metals during ultrasonic assisted deformation via CP-FEM. Mater Lett 65:356–359
26. Siddiq A, Sayed TE (2012) Ultrasonic-assisted manufacturing processes: variational model and numerical simulation. Ultrasonics 52(4):521–529. https://doi.org/10.1016/j.ultras.2011.11.004
27. Hung J, Hung C (2005) The influence of ultrasonic-vibration on hot upsetting of aluminum alloy. Ultrasonics 43(8):692–698. https://doi.org/10.1016/j.ultras.2005.03.001
28. Eaves AE, Smith AW, Waterhouse WJ, Sansome DH (1975) Review of the application of ultrasonic vibrations to deforming metals. Ultrasonics 13(4):162–170
29. Nevill GE, Brotzen FR (1957) The effect of vibrations on the static yield strength of a low-carbon steel. Proceeding-American Society for Testing Material. ASTM, Philadelphia, pp 751–754
30. Kempe W, Kroner E (1956) Dislocation damping of aluminum single crystals at room temperature. Z Met 47:302–304
31. Siegert K, Mock A (1996) Wire drawing with ultrasonically oscillating dies. J Mater Process Technol 60:657–660
32. Bagherzadeh S, Abrinia K, Liu Y, Han Q (2017) The effect of combining high-intensity ultrasonic vibration with ECAE process on the process parameters and mechanical properties and microstructure of aluminum 1050. Int J Adv Manuf Technol 88(1–4): 229–240
33. Mousavi SAAA, Feizi H, Madoliat R (2007) Investigations on the effects of ultrasonic vibrations in the extrusion process. J Mater Process Technol 187-188:657–661
34. Lou Y, He JS, Chen H, Long M (2017) Effects of vibration amplitude and relative grain size on the rheological behavior of copper during ultrasonic-assisted microextrusion. Int J Adv Manuf Technol 89(5–8):2421–2433

Publisher's Note